

Neutron and synchrotron X-ray diffraction study of the structures and dehydration behaviors of ramsdellite and “groutellite”

JEFFREY E. POST^{1,*} AND PETER J. HEANEY²

¹Department of Mineral Sciences, Smithsonian Institution, Washington, D.C. 20560-0119, U.S.A.

²Department of Geosciences, 309 Deike, Pennsylvania State University, University Park, Pennsylvania 16802, U.S.A.

ABSTRACT

The crystal structure of ramsdellite, MnO_2 , was refined using time-of-flight powder neutron diffraction data and the Rietveld method in order to assess the effects of reduction in cathodic battery materials. For the first time, we present a refined structure for “groutellite,” a heretofore poorly characterized phase with ideal formula $(\text{Mn}_{0.5}^{4+}\text{Mn}_{0.5}^{3+})\text{O}_{1.5}(\text{OH})_{0.5}$. “Groutellite” is generated synthetically as an intermediate compound during the reduction of ramsdellite to groutite (MnOOH), and it also occurs as an intergrowth in certain natural specimens of ramsdellite. The Jahn-Teller distortions in “groutellite” are confined to the **a-c** plane, and they result in a 6.8% unit-cell volume increase relative to ramsdellite. The Mn–O bond lengths refined for “groutellite” are consistent with the replacement of half of the Mn^{4+} and O^{2-} in ramsdellite by Mn^{3+} and $(\text{OH})^-$, respectively. In addition, the high-temperature behaviors of ramsdellite and “groutellite” were investigated by temperature-resolved synchrotron powder X-ray diffraction from 298 to 720 K. Rietveld refinements revealed a gradual thermal expansion of the groutellite structure to ~450 K. At higher temperatures, the unit-cell volume gradually decreased, primarily as a result of a decrease in *c*.

INTRODUCTION

Ramsdellite is one of two naturally occurring crystalline polymorphs of MnO_2 . Although pyrolusite is more common, ramsdellite can be locally abundant in oxidized zones of Mn-rich deposits subjected to low-temperature aqueous alteration (Ostwald 1984). A third MnO_2 phase, nsutite ($\gamma\text{-MnO}_2$), represents a disordered intergrowth of ramsdellite and pyrolusite (Turner and Buseck 1983). Nsutite and its synthetic analogue, electrolytic Mn dioxide (EMD), are the primary cathode materials used in both lithium and alkaline batteries (Ruetschi 1984; Paik et al. 2001).

Byström determined in 1949 that ramsdellite is isostructural with diaspore. It is constructed of double chains of edge-sharing Mn–O octahedra, and these chains share corners to form a framework with tunnels having rectangular cross-sections, measuring 1×2 octahedra on a side (Fig. 1). Pyrolusite, by contrast, has the rutile structure, consisting of single octahedral chains linked to form tunnels with square cross-sections measuring 1 octahedron on a side. In nsutite and EMD, ramsdellite and pyrolusite intergrow via the common single octahedron tunnel component. Battery-active EMD appears to exhibit two styles of structural disorder: (1) de Wolff defects, which include the random intercalation of ramsdellite-like and pyrolusite-like slabs as described above, and (2) micro-twinning of the ramsdellite structure with (021) and/or (061) as the composition planes (Chabre and Pannetier 1995; MacLean and Tye 1996).

As an alkaline battery discharges, Zn is oxidized at the anode and protons are transferred to (or in the materials science argot, inserted into) the Mn oxide at the cathode. Natural nsutite and

synthetic EMD are employed as cathodic battery materials because their tunnel topologies enable rapid solid-state diffusion of protons, and also because Mn can adopt multiple valence states (Balachandran et al. 2002). The electrochemical process entails the partial reduction of the cathodic material, and when Mn^{4+} in ramsdellite is reduced to Mn^{3+} , H^+ , or Li^+ will occupy sites within the 1×2 tunnels to maintain charge balance (Zachau-Christiansen et al. 1994; Chabre and Pannetier 1995; MacLean and Tye 1996).

The protonation of ramsdellite and pyrolusite generates the minerals groutite and manganite, respectively, both of which have the formula MnOOH . In addition, half-way along the ramsdellite-groutite join is a stable or metastable phase called “groutellite” by Klingsberg and Roy (1959), who first observed its appearance during the experimental reduction of ramsdellite to groutite (MnOOH). (“Groutellite” has not been approved as a mineral by the Commission on New Minerals and Mineral Names of the International Mineralogical Association, but because of historical convention, and prominent usage in the materials science literature, we will use the term without quotations hereafter.) Klingsberg and Roy (1959) suggest that groutellite exhibits the 2×1 structure of ramsdellite (and groutite), but that OH anions replace half of the O anions in an ordered fashion, leading to the formula $\text{MnO}_{1.5}(\text{OH})_{0.5}$. Interestingly, these authors did not observe the formation of groutellite during the reverse reaction as groutite was oxidized to ramsdellite.

The first reference to a natural occurrence of groutellite is found in Fleischer et al. (1962), who based their interpretation on weak reflections in precession photographs of ramsdellite crystals from Mexico. More recently, Post and Ross (1989) and MacLean et al. (1995) report X-ray powder diffraction evidence for natural groutellite intergrowths within samples of ramsdel-

* E-mail: post.jeffrey@nmnh.si.edu

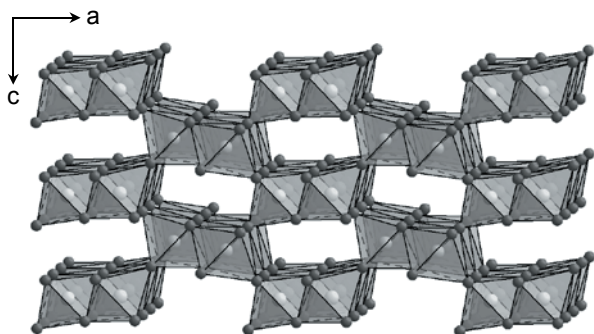


FIGURE 1. Polyhedral representation of the ramsdellite structure, projected approximately along *b*.

lite from New Mexico (Fig 2). MacLean et al. (1995) ascribe an OH-bending mode at 3398 cm^{-1} in infrared spectra of the New Mexican material to the inclusion of groutellite.

The relationships among the electrochemical reactivity, the disposition of H, and the MnO_2 defect structures in this system are poorly understood, but the presence of structural and chemical disorder is of integral importance to the effectiveness of these materials in batteries (MacLean et al. 1995; Paik et al. 2001). Highly crystalline ramsdellite, for example, has considerably lower reduction potential values than synthetic EMD. In addition, EMD generally contains $\sim 4\text{ wt}\%$ structural water (Tvarusko 1964), but the water locations remain an active area of study. Ruetschi and Giovanoli (1988) have proposed that H^+ in EMD structures occupies vacant Mn sites (as so-called Ruetschi protons), and also that the H^+ resides in the tunnels near reduced Mn^{3+} cations (Coleman protons). The typically poor crystallinity of EMD has hindered efforts to determine an accurate structure by diffraction methods (Chabre and Pannetier 1995).

A complete understanding of the ramsdellite and groutellite structures and their thermal behaviors may clarify the physical and chemical properties of EMD battery materials. Following the initial structure determination of Byström (1949), Fong et al. (1994) reported a Rietveld refinement for synthetic ramsdellite using powder neutron diffraction data, but details of their analysis seem problematic. For example, their calculated Mn-O distances exhibit an improbable range of 1.815 to 1.973 Å.

Here we report the most precise description of the ramsdellite structure to date, and we present the first structure solution and refinement of groutellite, as derived from a Rietveld refinement using powder neutron and synchrotron X-ray diffraction data. To the extent that groutellite serves as a natural analog to reduced EMD, these results yield significant insights into the structural changes to EMD after it has accommodated H^+ or Li^+ cations during electrochemical reduction during battery discharge. When EMD is prepared for use as a cathodic material in batteries, the compound must be heated to remove structural water. This process typically induces a partial transformation of ramsdellite to pyrolusite (Zachau-Christiansen et al. 1994). Therefore, we have also used real-time, temperature-resolved synchrotron X-ray diffraction data in conjunction with Rietveld refinements to investigate the behavior of the ramsdellite and groutellite structures from room temperature to 720 K. In this temperature range, groutellite oxidizes and dehydrates to ramsdellite, which subsequently transforms to pyrolusite.

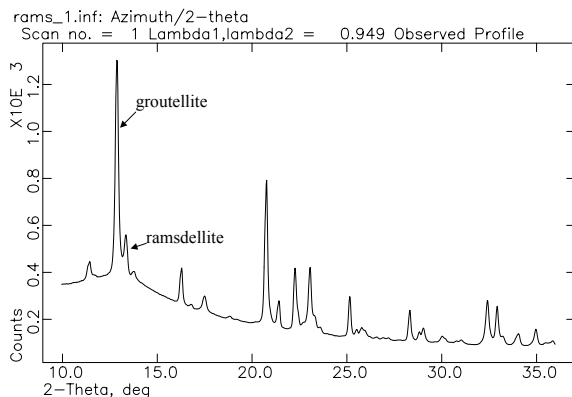


FIGURE 2. Powder X-ray diffraction pattern of sample from Lake Valley, New Mexico, showing the presence of ramsdellite and groutellite.

EXPERIMENTAL METHODS

Data collection

Diffraction data were collected using splintery, lath-like crystals removed from a ramsdellite specimen (NMNH no. 106192) from Lake Valley, New Mexico. Electron microprobe analyses showed only Mn and O, and bulk water analyses by the Penfield method yielded 2.11 wt% total water. Separate samples used for the X-ray and neutron diffraction experiments were ground in agate mortars to particle sizes below 400 mesh. A $\sim 10\text{ g}$ sample was loaded into a cylindrical vanadium sample container for neutron diffraction data collection. The samples for the X-ray diffraction study were loaded into 0.5 mm quartz-glass capillaries.

The room temperature time-of-flight neutron diffraction experiment was performed at the Manuel Lujan, Jr. Neutron Scattering Center at the Los Alamos National Laboratory. Data were collected for 2 h using the high intensity powder diffractometer (HIPD) with four detector banks centered at $\pm 90^\circ 2\theta$ and $\pm 153.4^\circ 2\theta$.

The X-ray diffraction data were collected at beam line X7B of the National Synchrotron Light Source (NSLS), Brookhaven National Laboratory (BNL). For the high-temperature experiment, the sample was heated from 298 to 720 K, at 2.9 K/min, using a Blake Instruments furnace with a Pt-13%Rh coiled wire yoke encased in ZrO_2 cement (Brown et al. 1973). The temperature was varied with an Omega controller and monitored with a Chromel-Alumel thermocouple located $\sim 2\text{ mm}$ from the specimen. The actual sample temperature was determined for the range 298 to 1273 K with a variety of melting transitions and by placement of an additional thermocouple in the sample position. The highly linear relationship between the observed and actual temperatures ($r^2 = 0.983$) allowed us to calculate a calibration curve with an estimated error of $\pm 5\text{ K}$ for a given temperature. The X-ray wavelengths used were 0.9492 Å for the 298 K experiment and 0.9370 Å for the heating experiment.

Intensities for the room temperature Rietveld refinement of groutellite were collected using a 120 s exposure with a $20 \times 40\text{ cm}$ Fuji imaging plate mounted perpendicular to the incoming beam at a distance of 217.2 mm. The exposed plate was scanned by a Fuji BAS2000 reader, which yielded a nominal pixel size of $0.1 \times 0.1\text{ mm}^2$ (2048×4096 pixels) and a dynamic range of 10^4 . Additional details for this procedure are provided by Norby (1997).

The temperature-resolved data were collected in air as a series of 120 s exposures with a MAR345 full imaging plate detector. The temperature was increased continuously at a rate of 2.9 K/min and measurements were obtained every $\sim 11\text{ K}$; due to down time for repositioning of the sample and reading the imaging plate, each exposure represents a temperature range of $\sim 5\text{ K}$. During each exposure the sample was rotated through a 90° angle. Any preferred orientation of the powder should have been eliminated through a combination of the specimen rotation, use of a capillary sample holder, and full intensity integration of the diffraction rings, as obtained using the program Fit2D (Hammersley et al. 1996) with a polarization factor of 0.93.

The transmission infrared spectroscopy data were collected using a Bio-Rad

FTS3000 spectrometer with an attached UMA-500 microscope that uses an MCT detector. The room-temperature spectra were collected using KBr pellets (~2 mg sample to 250 mg KBr). The high-temperature study was carried out using a Linkham Scientific Instruments FTIR600 heating stage with a TMS94 controller. Approximately 2 mg of the ramsdellite powder dispersed in water was evaporated onto a BaF₂ disc, which was loaded into the heating stage. The heating stage sample chamber was sealed top and bottom with BaF₂ windows and purged throughout the heating experiment with dried and CO₂-scrubbed air. The sample was heated from 298 to 373 K at 10 K per minute, and from 373 to 573 K at 5 K per minute. Above 373 K, spectra were collected every 20 K after the sample was at temperature for 5 minutes. Background spectra were collected from a sample-free area of the BaF₂ disc. The temperature was monitored with a platinum resistor sensor to a stated accuracy of ± 0.1 °C, and measurements made for a variety of known melting and solid-state phase transitions showed the thermocouple temperature was accurate to within ± 2 K.

Structure refinements

All refinements were performed with the General Structure Analysis System (GSAS) program of Larson and Von Dreele (2001). The starting atom coordinates for the powder X-ray and neutron diffraction room-temperature refinements were taken from Byström (1949). For the neutron refinement, the data from the +90° detector bank were used. The backgrounds for the X-ray and neutron diffraction patterns were fit using a linear interpolation function and cosine series function, respectively. Peak profiles in the neutron data were approximated using the profile convolution function of Von Dreele et al. (1982), and the X-ray peaks were modeled with a pseudovoigt profile function as parameterized by Thompson et al. (1987) with asymmetry corrections by Finger et al. (1994) and microstrain anisotropic broadening terms by Stephens (1999).

During refinement of the atom positions, soft constraints were applied to the Mn-O distances (constrained to 1.90 Å, with standard deviation of 0.05 Å), and the weighting factor was gradually reduced, and eventually eliminated in successive cycles.

The Rietveld refinements revealed that the sample examined by neutron diffraction consisted of ~75% ramsdellite and 25% groutellite. The sample used for the X-ray refinement of groutellite was ~77% groutellite, 18% ramsdellite, and 5% pyrolusite, and the sample used for the X-ray heating study initially comprised ~57% groutellite, 26% ramsdellite, and 17% pyrolusite. In all cases, unit-cell and profile parameters, atom position, and displacement factors were refined for ramsdellite and groutellite. Only the unit-cell and profile parameters were refined for the pyrolusite sample. It was not possible to refine precise atom positions or locate H atoms for groutellite using the neutron diffraction data because of the relatively small fraction of groutellite in the sample. We were unsuccessful in separating a quantity of groutellite-rich sample sufficient for collecting high-quality powder neutron diffraction data.

TABLE 1. Final Rietveld refinement parameters for ramsdellite and groutellite

	Ramsdellite (neutron)	Groutellite (X-ray)
Space group	<i>Pnma</i>	<i>Pnma</i>
Refinement		
No. of data points	3926	1823
No. of reflections	2525	207
Diffraction range (<i>d</i>)	3.11–0.45 Å	6.75–1.0 Å
No. of variables	38	84
<i>R</i> (<i>F</i> ²)	0.044	0.048
<i>R</i> _{wp}	0.043	0.028
χ^2	1.63	0.128

The final refinement parameters for the ramsdellite analysis using powder neutron data and those for the groutellite analysis using powder X-ray data are listed in Table 1. The refined unit-cell parameters at 298 K are listed in Table 2. The atomic positions are included in Table 3, and corresponding bond distances are reported in Table 4. The final observed, calculated, and difference powder diffraction patterns resulting from the Rietveld refinements are plotted in Figure 3. Rietveld refinements were also performed for a series of XRD patterns from room temperature to near the ramsdellite to pyrolusite transition temperature. These refinements revealed changes with temperature that are discussed below.

Estimation of errors

In our Rietveld analyses using synchrotron X-ray diffraction data collected with the Fuji imaging plate, the final χ^2 values typically fell below 1.00. The reduced χ^2 is calculated by GSAS as $\chi^2 = M/(N_{\text{obs}} - N_{\text{var}})$, where N_{obs} is the number of observed intensities and N_{var} is the number of refined variables. M is the function minimized during the refinement and is defined as $M = \sum w(I_o - I_c)^2$, where I_o and I_c are the observed and calculated intensities at a given value of 2θ and the weighting factor w is equal to the inverse of the square of the estimated standard deviation (i.e., $w = 1/(\text{e.s.d.})^2$) (Larson and Von Dreele 2001). In our data sets, the e.s.d. for a given 2θ was arbitrarily calculated as the square root of the intensity. Because an amorphous component contributed very high background intensities to our patterns, the calculated e.s.d.s for our patterns were unreasonably large. Consequently,

TABLE 2. Unit-cell parameters and volume at 298 K for ramsdellite (neutron), groutellite (X-ray), and groutite

	<i>a</i> (Å)	<i>b</i> (Å)	<i>c</i> (Å)	<i>V</i> (Å ³)
Ramsdellite	9.2734(7)	2.8638(2)	4.5219(3)	120.09(2)
Groutellite	9.5155(3)	2.8644(1)	4.7061(2)	128.270(7)
Groutite*	10.667(1)	2.871(1)	4.554(1)	139.47

* Kohler et al. (1997).

TABLE 3. Atomic coordinates and isotropic displacement factors for ramsdellite and groutellite at 298 K

Atom	<i>x</i>	<i>y</i>	<i>z</i>	Site occupancy factor	<i>U</i> _{iso}
ramsdellite (<i>Pnma</i>)					
Mn1	0.1332(5)	0.25	0.0258(7)	1.0	0.0021(5)
O1	0.9655(3)	0.25	0.7838(4)	1.0	0.0041(5)
O2	0.2796(2)	0.25	0.3201(5)	1.0	0.0034(4)
groutellite (<i>Pnma</i>)					
Mn1	0.1416(2)	0.25	0.0407(3)	1.0	0.0393(4)
O1	0.9577(6)	0.25	0.7819(9)	1.0	0.046(1) [†]
O2	0.2791(6)	0.25	0.342(1)	1.0	0.046(1) [†]

* Isotropic displacement factors for O1 and O2 in groutellite were constrained to be equal.

TABLE 4. Selected bond distances (Å) for ramsdellite and groutellite at 298 K

	Ramsdellite	Groutellite
Mn1-O1	1.905(3) × 2	1.908(4) × 2
Mn1-O1	1.901(4)	2.132(6)
Mn1-O2	1.889(3) × 2	1.868(4) × 2
Mn1-O2	1.901(5)	1.931(6)
<Mn-O>	1.898	1.936
O1-O1	2.506(3) × 2	2.629(8) × 2
O1-O2	2.486(3)	2.452(8)

the weighting factors w were unreasonably low, generating values for χ^2 that consistently fell below unity.

Our inspection of the variation in the estimated standard deviation as a function of the scattering angle revealed no systematic dependence on 2θ . Consequently, the minimization calculations performed by GSAS were not biased by the unrealistic e.s.d.s. As a result, the final χ^2 values calculated during our analyses of the synchrotron X-ray diffraction data are meaningful as relative measures of the goodness of fit, albeit not as absolute measures. However, the reasonable bond distances and the low values for R_{wp} and R_{Bragg} provided independent measures of the accuracy of the final refined structure. As is often the case, the standard deviations calculated by GSAS for the lattice parameters are lower than the true errors (Post and Bish 1989). We present the errors calculated by GSAS in the tables and figures of this paper with the understanding that the actual errors may be more than an order of magnitude higher than the calculated deviations.

DISCUSSION

Ramsdellite

The results of the refinement of the ramsdellite structure using powder neutron data agree reasonably well with the structure reported by Byström (1949), but provide improved precision for the bond distances. The O atoms form a nearly regular octahedron around the Mn atoms at distances ranging from 1.889 to 1.905 Å (Table 4), and the mean Mn-O distance of 1.898 Å

compares well with the Mn⁴⁺-O value of 1.89 Å measured for pyrolusite (Baur 1976). The Mn cations are displaced slightly off center, probably due to cation-cation repulsions between adjacent octahedra. Similar displacements have been reported for other phases having double octahedral chains, such as the hollandite structure (e.g., Post et al. 1982). The O-O distance along the shared octahedral edges are 2.486 and 2.506 Å.

Groutellite

The room-temperature refinement of the groutellite structure reveals that the Mn octahedra are distorted relative to those in ramsdellite (Table 4.) The Mn-O distances range from ~1.87 to 2.13 Å, and the mean value of 1.94 Å is significantly larger than that of ramsdellite. The elongated axial Mn-O bond lengths (2.13 and 1.93 Å) relative to the equatorial distances (1.91 and 1.87 Å) are characteristic of Jahn-Teller distortion and strongly indicate that some trivalent Mn occupies the octahedral site. Also, one of the O-O distances along the shared octahedral edges is lengthened and one is shortened, relative to those in ramsdellite (Table 4). Using the bond lengths of Shannon (1976) for Mn⁴⁺-O and Mn³⁺-O of 1.89 and 2.005 Å, respectively, and the observed mean Mn-O distance of 1.94 Å, we can calculate that approximately 43% of the Mn in groutellite must be Mn³⁺. As is discussed below, the reduced charge at the octahedral site is offset by the replacement of some of the O atoms by OH⁻ anions, or in the case of some battery materials by the addition of Li⁺ cations into the tunnels.

Assuming that the reduction of Mn⁴⁺ to Mn³⁺ in our natural ramsdellite sample is accompanied by substitution of OH⁻ for O²⁻, the chemical formula for groutellite is (Mn_{0.57}⁴⁺, Mn_{0.43}³⁺)O_{1.57}(OH)_{0.43}, and the average oxidation state for the Mn is +3.57. Paik et al. (2001) determined average Mn oxidation states of +3.5 and +3.3 for synthetic ramsdellite reduced at 293 and 323 K, respectively. The difference between our derived formula and the ideal formula proposed by Klingsberg and Roy (1959) probably falls within the uncertainties of our refinement and/or bond length calculations.

We were unable to locate the partially occupied H⁺ cation site during our refinement. A recent first-principles study of H-insertion in Mn oxides (Balachandran et al. 2002) concluded that the H⁺ in the ramsdellite structure is most probably bonded to O2.

The unit-cell volume of groutellite is 6.8% greater than that of ramsdellite, with the expansion occurring almost equally in the a and c dimensions; b is not significantly different in the two phases. This observation is consistent with the increase resulting from the Jahn-Teller axial distortion of the Mn-O octahedra in groutellite, as the distortion is confined to the a - c plane.

The composition of groutellite nominally lies halfway along the join between ramsdellite and groutite. Based on the consistency of its unit-cell parameters for a variety of mineral specimens and synthetic preparations, groutellite appears to be a distinct intermediate phase. To date, there is no evidence to suggest that groutellite represents a continuous range of compositions that might constitute a ramsdellite-groutite solid solution series. Nevertheless, the reduction of ramsdellite to groutite does not require a major change in structure, as the two phases are topologically identical, but the Mn-O octahedra of groutite are significantly rotated with respect to those of ramsdellite (Fig. 4).

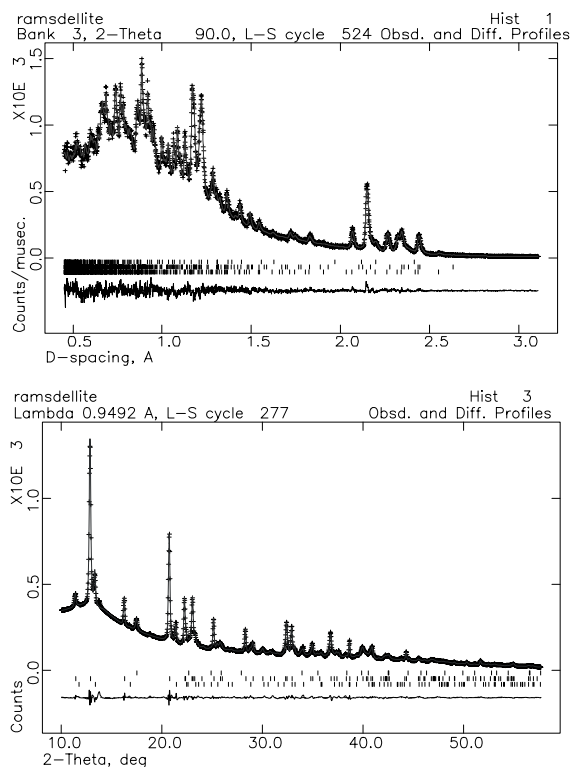


FIGURE 3. Final observed (crosses), calculated (solid line), and difference (lower) powder diffraction patterns for the Rietveld refinement of (a) ramsdellite and groutellite using powder neutron diffraction data, and (b) groutellite and ramsdellite using synchrotron X-ray diffraction data.

Comparison of the ramsdellite and groutellite structures (Fig. 4) reveals an axial elongation of the Mn-O octahedra in groutellite, but only a slight octahedral rotation.

The unit-cell parameters for groutellite and ramsdellite are

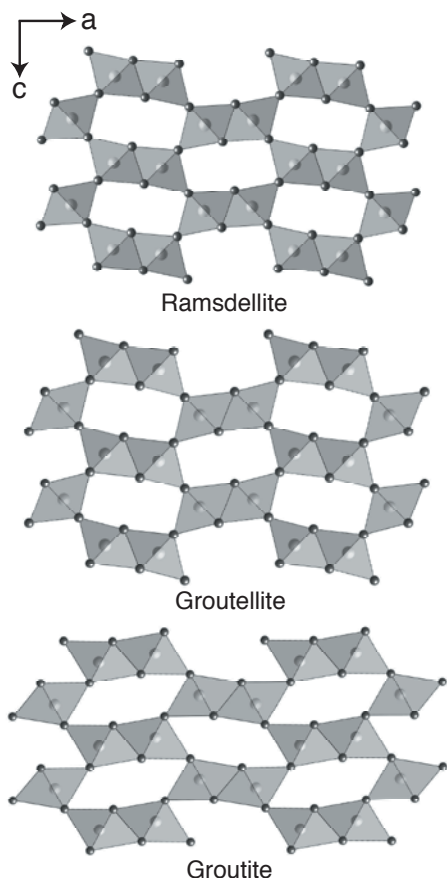


FIGURE 4. Polyhedral representations of the groutite (Kohler et al. 1997), ramsdellite, and groutellite structures.

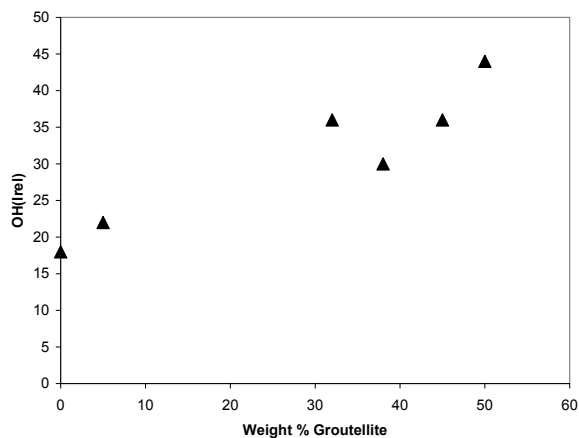


FIGURE 5. Plot of the observed intensities (peak heights, relative to the strongest Mn-O stretch band) of the infrared spectra OH-stretch absorption line vs. groutellite weight percent, as determined by Rietveld refinements.

listed in Table 2 along with those of groutite, and whereas the a dimension of groutellite has a length that is intermediate between those of ramsdellite and groutite, the c parameter of groutellite is significantly longer than that of either groutite or ramsdellite. Apparently, then, as ramsdellite is reduced, its structure initially accommodates the Mn^{3+} and OH^- substitutions by expanding a and c , with only slight octahedral rotation. The composition of groutellite likely represents the maximum degree of reduction that can be accommodated by this mechanism. Any additional reduction requires the more severe octahedral twist that is observed in groutite (Kohler et al. 1997; MacLean and Tye 1996). The energy required to initiate the groutite twist probably is the barrier that stabilizes the groutellite structure. This interpretation is consistent with the two-step process proposed by Maskell et al. (1981) for electrochemical reduction of $\gamma\text{-MnO}_2$, proceeding first from MnO_2 to $\text{MnOOH}_{0.5}$ and then to MnOOH .

Infrared spectra were collected from a series of ramsdellite samples from Lake Valley, New Mexico that exhibited a range of ramsdellite:groutellite compositions. In Figure 5 we plot the observed intensities (peak heights, relative to the strongest Mn-O stretch band) of the OH stretch absorption line ($\sim 3398\text{ cm}^{-1}$) vs. the weight percent groutellite, as determined by Rietveld refinements. The positive and approximately linear correlation between OH and groutellite concentration supports the above assumption that for these samples, reduction of Mn^{4+} to Mn^{3+} during the transformation of ramsdellite to groutellite is coupled with substitution of OH^- for O^{2-} anions.

Heating experiments

Our synchrotron X-ray diffraction data showed that groutellite completely transformed to ramsdellite in air in the temperature range 530 to 600 K (Fig. 6). Rietveld refinements revealed a gradual thermal expansion of the groutellite structure to ~ 530 K (Fig. 7). At higher temperatures, the unit-cell volume gradually decreased. The volume decrease is likely related to the oxidation of Mn^{3+} to the smaller Mn^{4+} , and this conclusion is supported by the Rietveld refinement results indicating a steady shortening of the axial Mn-O distances above ~ 500 K, e.g., from 2.14 Å at 500 K to 2.05 Å at 580 K. Furthermore, the temperature-resolved IR

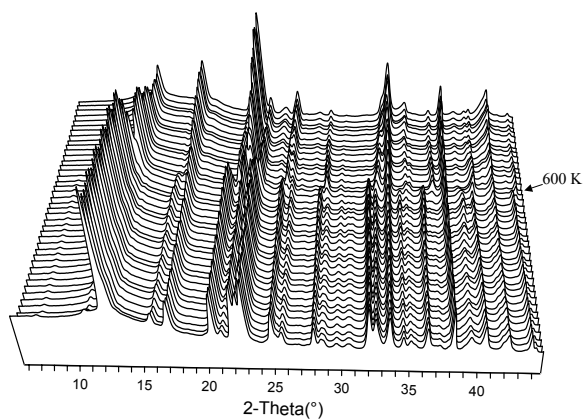


FIGURE 6. Synchrotron XRD patterns for groutellite/ramsdelite sample vs. temperature, 298 to 720 K.

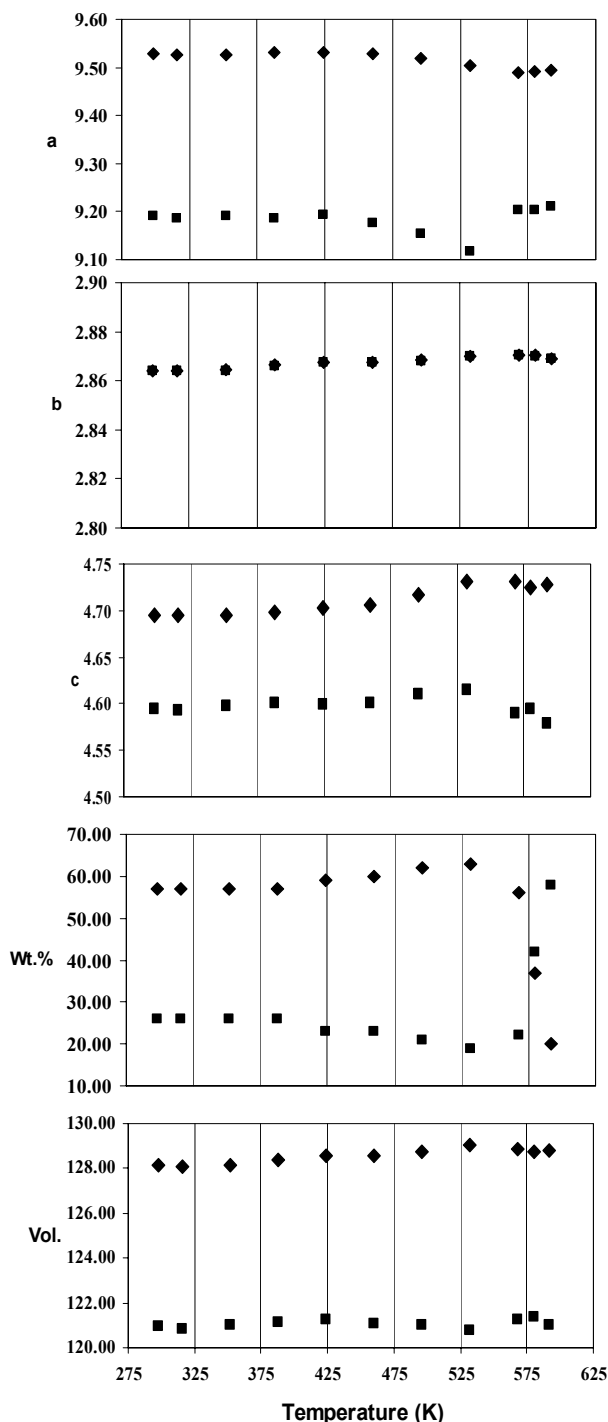


FIGURE 7. Plots of groutellite (diamonds) and ramsdellite (squares) unit-cell parameters and wt% groutellite vs. temperature (K).

spectra show a decrease in the intensities of the OH bands in the region 3000–3600 cm^{-1} starting at ~513 K and continuing until they disappear at ~573 K (Fig. 8), indicating loss of H^+ as Mn is oxidized, and groutellite transforms to ramsdellite. The unit-cell volume for ramsdellite increased ~0.5 to 425 K, then decreased to ~530 K, and then appears to gradually increase

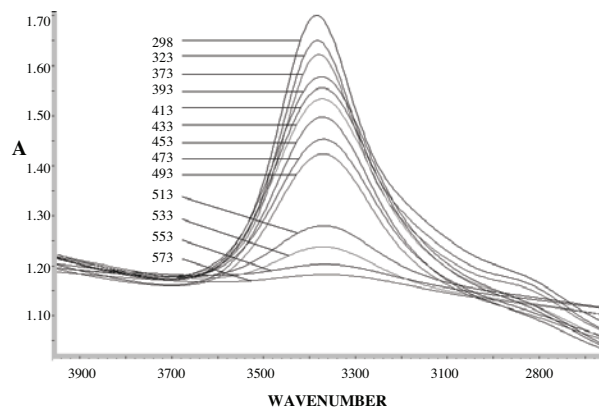


FIGURE 8. Temperature-resolved infrared spectra for a ramsdellite/groutellite sample from Lake Valley heated from 298 to 573 K.

again. At ~425 K, the groutellite and ramsdellite *a* dimensions began a steady decline that continued until groutellite disappeared. The groutellite *c* parameter, on the other hand, increased continuously from RT to ~575 K, with a marked acceleration above 530 K, and for ramsdellite the *c* dimension increased to ~530 K, and then decreased.

Above ~590 K ramsdellite started to transform into pyrolusite, but at the maximum temperature of our experiment, 720 K, some ramsdellite remained. Because the observed changes in our heating experiments were not reversible in air, the choice of heating rate might affect the lowest temperature at which these transformation events were observed. Klingsberg and Roy (1959), however, report that ramsdellite from Chisholm, Minnesota, U.S.A. heated for four days at 589 K was unchanged, while heating at 586 K for 14 days resulted in the appearance of a trace of pyrolusite. Ramsdellite from Lake Valley, New Mexico, U.S.A. heated by Fleischer et al. (1962) at 583 K for 5 days was converted almost entirely to pyrolusite. These results suggest that regardless of the heating rate, ramsdellite is stable to at least ~580 K, and this value is close to the temperature at which we first observed groutellite changing to pyrolusite.

The change in the refined weight percent of groutellite in ramsdellite/groutellite mixtures with increasing temperature (Fig. 7) reveals that the fraction of groutellite actually increases through the temperature range of ~420 to 530 K from 57% to 63%, at the expense of ramsdellite. Evidently, as the sample is heated in that temperature range, some of the Mn^{4+} in ramsdellite is reduced to Mn^{3+} with coupled replacement of some of the O^{2-} by OH^- . Above ~530 K, the reaction is reversed as groutellite starts back-reacting to ramsdellite. We confirmed this behavior by using Rietveld quantitative methods to compare the relative abundance of ramsdellite and groutellite for several New Mexico ramsdellite samples before and after they were heated in an oven to 423 K for 2 to 24 h. In all cases, the fraction of groutellite increased and that of ramsdellite decreased, and the increase in groutellite content was consistently greater for samples heated for 24 h. On the other hand, when the powders were heated 50 K higher, to 473 K for 24 h, all of the groutellite had transformed into ramsdellite.

ACKNOWLEDGMENTS

Support for this research was provided by NSF grant NSF EAR01-25908. Brookhaven National Laboratory and the National Synchrotron Light Source are supported under contract DE-AC02-98CH10886 with the U.S. Department of Energy by its Division of Chemical Sciences, Office of Basic Energy Research. Crystal structure drawings were produced using CrystalMaker 5.0 by D. Palmer. We gratefully acknowledge R. Isaac and M. Jenkins for their valuable assistance with the IR heating experiments, R. Von Dreele for helping with the neutron data collection, J. Hanson for his assistance with the synchrotron experiments, and D. Ross for assistance with the powder XRD study. We also thank G. Russman and an anonymous reviewer for helpful comments.

REFERENCES CITED

- Balachandran, D., Morgan, D., and Ceder, G. (2002) First principles study of H-insertion in MnO₂. *Journal of Solid State Chemistry*, 166, 91–103.
- Baur, W.H. (1976) Rutile-type compounds. V. Refinement of MnO₂ and MgF₂. *Acta Crystallographica*, B32, 2200–2204.
- Brown, G.E., Sueno, S., and Prewitt, C.T. (1973) A new single-crystal heater for the precession camera and four-circle diffractometer. *American Mineralogist*, 58, 698–704.
- Byström, A.M. (1949) The crystal structure of ramsdellite, an orthorhombic modification of MnO₂. *Acta Scandinavica*, 3, 163–173.
- Chabre, Y. and Pannetier, J. (1995) Structural and electrochemical properties of the proton/ γ -MnO₂ system. *Progress in Solid State Chemistry*, 23, 1–130.
- Finger, L.W., Cox, D.E., and Jephcoat, A.P. (1994) A correction for powder diffraction peak asymmetry due to axial divergence. *Journal of Applied Crystallography*, 27, 892–900.
- Fleischer, M., Richmond, W.E., and Evans, Jr., H. (1962) Studies of the manganese oxides. V. ramsdellite, MnO₂, an orthorhombic dimorph of pyrolusite. *American Mineralogist*, 47, 47–66.
- Fong, C., Kennedy, B.J., and Elcombe, M.M. (1994) A powder neutron diffraction study of λ and γ manganese dioxide and of LiMn₂O₄. *Zeitschrift für Kristallographie*, 209, 941–945.
- Hammerley, A.P., Svensson, S.O., Hanfland, M., Fitch, A.N., and Hausermann, D. (1996) Two-dimensional detector software: From real detector to idealised image or two-theta scan. *High Pressure Research*, 14, 235–248.
- Klingsberg, C. and Roy, R. (1959) Stability and interconvertibility of phases in the system Mn-O-OH. *American Mineralogist*, 44, 819–838.
- Kohler, T., Armbruster, T., and Libowitzky, E. (1997) Hydrogen bonding and Jahn-Teller distortions in groutite, α -MnOOH, and manganite, γ -MnOOH, and their relations to the manganese dioxides ramsdellite and pyrolusite. *Journal of Solid State Chemistry*, 133, 486–500.
- Larson, A.C. and Von Dreele, R.B. (2001) GSAS-General Structure Analysis System. Los Alamos National Laboratory Report No. LAUR 86–748.
- MacLean, L.A.H. and Tye, F.L. (1996) The structure of fully H-inserted γ -manganese dioxide compounds. *Journal of Solid State Chemistry*, 123, 150–160.
- MacLean, L.A.H., Poinson, C., Amarilla, J.M., Le Cras, F., and Strobel, P. (1995) Electrochemical behavior of natural and synthetic ramsdellite. *Journal of Material Chemistry*, 5, 1183–1189.
- Maskell, W.C., Shaw, J.E.A., and Tye, F.L. (1981) Manganese dioxide electrode – IV. Chemical and electrolytical reduction of an electrolytic γ -MnO₂. *Electrochimica Acta*, 26, 1403–1410.
- Norby, P. (1997) Synchrotron powder diffraction using imaging plates: Crystal structure determination and Rietveld refinement. *Journal of Applied Crystallography*, 30, 21–30.
- Ostwald, J. (1984) Some observations on the genesis of nsutite. *Neues Jahrbuch für Mineralogie-Monatshefte*, H9, 385–392.
- Paik, Y., Osegovic, J.P., Wang, F., Bowden, W., and Grey, C.P. (2001) ²H MAS NMR studies of the manganese dioxide tunnel structures and hydroxides used as cathode materials in primary batteries. *Journal of the American Chemical Society*, 123, 7564–7573.
- Post, J.E. and Bish, D.L. (1989) Rietveld refinement of crystal structures using powder X-ray diffraction data. In D.L. Bish and J.E. Post, Eds., *Reviews in Mineralogy: Modern Powder Diffraction*, 20, 277–308. The Mineralogical Society of America, Washington, D.C.
- Post, J.E. and Ross, D.R. (1989) Rietveld refinements of two coexisting ramsdellite phases. *EOS*, 70, 352.
- Post, J.E., Von Dreele, R.B., and Buseck, P.R. (1982) Symmetry and cation displacements in hollandites: structure refinements of hollandite, cryptomelane, and priderite. *Acta Crystallographica*, B38, 1056–1065.
- Ruetschi, P. (1984) Cation-vacancy model for MnO₂. *Journal of the Electrochemical Society*, 131, 2737–2743.
- Ruetschi, P. and Giovanoli, R. (1988) Cation vacancies in MnO₂ and their influence on electrochemical reactivity. *Journal of the Electrochemical Society*, 135, 2663–2669.
- Shannon, R.D. (1976) Revised effective ionic radii and systematic studies of interatomic distances in halides and chalcogenides. *Acta Crystallographica*, A32, 751–767.
- Stephens, P.W. (1999) Phenomenological model of anisotropic peak broadening in powder diffraction. *Journal of Applied Crystallography*, 32, 281–289.
- Thompson, P., Cox, D.E., and Hastings, J.B. (1987) Rietveld refinement of Debye-Scherrer synchrotron X-ray data from Al₂O₃. *Journal of Applied Crystallography*, 20, 79–83.
- Turner, S. and Buseck, P.R. (1983) Defects in nsutite (γ -MnO₂) and dry-cell battery efficiency. *Nature*, 304, 143–146.
- Tvarusko, A. (1964) Investigations of manganese oxides 1. Water content. *Journal of the Electrochemical Society*, 111, 125–131.
- Von Dreele, R.B., Jorgenseu, J.D., and Windsor, C.G. (1982) Rietveld refinement with spallation neutron powder diffraction data. *Journal of Applied Crystallography*, 15, 581–589.
- Zachau-Christiansen, B., West, K., Jacobsen, T., and Skaarup, S. (1994) Insertion of lithium into the manganese dioxides: pyrolusite and ramsdellite. *Solid State Ionics*, 70/71, 401–406.

MANUSCRIPT RECEIVED AUGUST 1, 2003

MANUSCRIPT ACCEPTED DECEMBER 15, 2003

MANUSCRIPT HANDLED BY PETER BURNS